CaRPOOL: A Pooled Calcium-Recording CRISPR Screening Platform Identifies CCR7 as a Modulator of Cellular Osmomechanosensing

Miao Ouyang[1,2], Jianhui Wang[1,2] and Ruilin Tian[1,2,*]

[1]SUSTech Homeostatic Medicine Institute, School of Medicine, Southern University of Science and Technology, Shenzhen 518055, China

[2]Key University Laboratory of Metabolism and Health of Guangdong, Southern University of Science and Technology, Shenzhen 518055, China

[*]Correspondence: tianrl@sustech.edu.cn (R.T.)

ABSTRACT

Cells must continuously sense and respond to environmental changes by translating physical and chemical cues into intracellular signals. However, systematic discovery of genes governing these sensory processes has been limited by the transient nature of signaling events and the low throughput of measurement assays. Here, we present CaRPOOL, a pooled, high-throughput genetic screening platform that integrates the calcium-activity recorder CaMPARI2 with CRISPR interference (CRISPRi), enabling stable capture of transient calcium signals for genome-scale functional screening. Using osmomechanical stimulation as a model, we demonstrate that CaMPARI2 photoconversion faithfully reports stimulus-dependent calcium responses and supports pooled fluorescence-activated cell sorting (FACS)-based screening. A CRISPRi library targeting membrane-associated genes identified both known and previously uncharacterized regulators of mechanotransduction, including the chemokine receptor CCR7. Mechanistic analyses revealed that CCR7 promotes osmomechanical calcium signaling through a PIEZO1-dependent Gαs-cAMP-PKA pathway, establishing it as a mechanosensitive GPCR. Notably, osmotic stress upregulated *CCR7* expression in immune cells and enhanced mechanical responsiveness, suggesting a role in immunomechanical adaptation. Together, these findings introduce a broadly applicable platform for high-throughput discovery of genes controlling dynamic

31 signaling responses and reveals a GPCR-ion channel crosstalk mechanism in
32 mechanotransduction with potential implications for immune cell mechanoadaptation.
33

INTRODUCTION

Cells continuously sense and respond to environmental stimuli, translating physical and chemical cues into intracellular signals that maintain homeostasis and guide development and adaptation [1-3]. These stimuli—including mechanical forces[4, 5], temperature[6, 7], light [8], and chemical ligands[9, 10]—are primarily detected by membrane proteins such as G protein-coupled receptors (GPCRs) and ion channels that act as molecular sensors coupling external inputs to intracellular signaling cascades[11]. The identification of these sensory molecules, along with their regulatory components that modulate receptor activity, localization, and downstream signaling, has been central to understanding how organisms perceive and adapt to their surroundings.

Genetic screening has been instrumental in uncovering key genes mediating cellular responses to environmental stimuli. A landmark example is the discovery of PIEZO1 as a mechanosensitive ion channel, achieved through systematic siRNA knockdown in mouse neuroblastoma cells followed by whole-cell patch-clamp recordings to measure mechanically activated currents in response to cell poking—a laborious process requiring manual electrophysiological analysis of hundreds to thousands of individually transfected cells[12]. Similarly, identification of TRPV1 as the capsaicin and heat receptor relied on expression cloning in HEK293 cells combined with calcium imaging of individual clones, an approach that required screening hundreds to thousands of cDNA pools one by one[6]. More recently, efforts have sought to scale sensory screens using automation and genetic arrays. A screen for cold-sensing receptors in *Caenorhabditis elegans* employed a custom real-time PCR thermocycler to deliver controlled temperature stimuli while monitoring calcium responses across arrayed mutants, ultimately identifying GLR-3 as a cold sensor[13]. Likewise, Xu et al. engineered a microfluidic platform that applied shear stress stimulation in 384-well format to identify the flow-responsive GPCR GPR68[14]. While these pioneering examples illustrate the power of genetic screening in sensory biology, they also underscore a persistent limitation: most rely on low-throughput readouts or specialized instrumentation that hinder large-scale, unbiased discovery.

The fundamental challenge lies in capturing transient signaling events—which typically last seconds to minutes—in a format compatible with pooled genetic screening, where millions of cells carrying different genetic perturbations must be analyzed simultaneously. Traditional real-time sensors require continuous observation during stimulation, making them incompatible with pooled screening workflows. Endpoint assays such as transcriptional reporters can work in pooled formats but miss the immediate signaling dynamics that define cellular sensing. Calcium signaling, which serves as a nearly universal readout of cellular activation across diverse stimuli, would be an ideal screening parameter if its transient dynamics could be stably recorded.

In this study, we developed CaRPOOL (Calcium-Recording Pooled screening platform), a high-throughput genetic screening platform that integrates a calcium-activity recorder with CRISPR screening, enabling systematic discovery of genes that govern cellular responses to external stimuli. Applying this platform to osmomechanical stimulation uncovered the chemokine receptor CCR7 as a previously unrecognized regulator of mechanotransduction that operates in a PIEZO1-dependent manner through the Gαs-cAMP-PKA signaling axis. By providing a broadly applicable approach for uncovering regulators of mechanosensation and other stimulus-responsive processes, this technology expands the toolkit for elucidating how cells perceive and translate environmental forces into biological function.

RESULTS

CaMPARI2 Enables High-Throughput Measurement of Calcium Responses to Osmotic Mechanical Stimulus

Various extracellular stimuli, such as changes in temperature, mechanical force, osmolarity, and pH, induce cellular responses that converge in elevated cytosolic calcium concentration. Therefore, calcium signaling can serve as a proxy to measure cellular responses to external stimuli. Calcium imaging using small-molecule probes such as Fluo-4 and Fura-2, or genetically encoded calcium sensors like GCaMP[15], is a widely used approach for real-time monitoring of intracellular Ca^{2+} dynamics. However, because calcium signals are transient and dynamic, these methods rely on fluorescence microscopy or plate readers, limiting their throughput to low- or medium-scale arrayed screens and making them unsuitable for pooled, high-throughput applications.

By contrast, calcium integrators provide a means to record transient calcium activity into a stable fluorescence readout. The Ca^{2+}-Activated Photoactivatable Ratiometric Integrator (CaMPARI) is a photoconvertible fluorescent protein that irreversibly switches its from green to red fluorescence under violet light, but only in the presence of elevated Ca^{2+} [16, 17]. This property allows the recording of cellular calcium activity during a defined illumination window into a stable, integrated fluorescence parameter—the red-to-green (R/G) ratio—which can be measured at single-cell resolution by flow cytometry, thus enabling pooled high-throughput screening. The higher the CaMPARI R/G ratio, the greater the accumulated Ca^{2+} during the illumination period, reflecting stronger cellular responses to a given stimulus (Figure 1A).

We sought to determine whether CaMPARI could be applied to high-throughput screening of cellular responses to mechanical stimulation. To deliver uniform mechanical stimulation to large populations of cells in a scalable manner, we employed osmotic mechanical stress. By altering extracellular osmolarity, cells undergo volume

changes and membrane deformation, generating mechanical force without the need for complex physical devices. This approach is commonly used to mimic mechanical stress in cellular systems. We selected HEK293T cells, a kidney-derived cell line, for these experiments because the kidney is a major organ involved in osmotic and mechanical sensation, and this cell line is well-established and easy to handle.

We first verified whether HEK293T cells generate calcium respond to osmotic mechanical stimulation. Cells were treated with a hypertonic solution containing sorbitol, a non-ionic osmolyte, or with a hypotonic solution prepared by diluting the culture medium with water. Using the calcium indicator GCaMP8f, we detected robust and osmolarity-dependent increases in cytosolic calcium concentration in HEK293T cells by both fluorescence imaging (Figures 1B-C) and microplate reader (Figures S1A-B), consistent with previous reports[18-21].

We then tested whether CaMPARI could report cellular responses to osmomechanical stimulation. To this end, we generated a HEK293T cell line stably expressing CaMPARI2, an improved version of CaMPARI. Cells were subjected to hypertonic or hypotonic treatments while being simultaneously exposed to violet light for 3 minutes. Both fluorescence microscopy and flow cytometry revealed significant increases in the CaMPARI2 red-to-green (R/G) ratios under hypertonic and hypotonic conditions compared to isotonic or no-violet light controls, with responses scaling in an osmolarity-dependent manner (Figures 1D-G). Notably, hypotonic stimulation elicited a stronger calcium response than hypertonic stress. Based on this observation, we selected a 1:1 H_2O-to-medium mixture as the osmomechanical stimulation condition for downstream experiments.

To exclude potential ionic effects, we prepared defined solutions composed only of sterile water, sucrose, and $CaCl_2$, with theoretical osmolarities approximating hypertonic (~700 mOsm/L), isotonic (~300 mOsm/L), and hypotonic (~150 mOsm/L) conditions. Comparable CaMPARI2 responses were observed under these conditions,

confirming that the calcium increases were primarily driven by osmotic pressure rather than ionic composition (Figure 1H).

In summary, these results demonstrate that HEK293T cells exhibit robust calcium response to both hypertonic and hypotonic stimulation and establish CaMPARI2 as a sensitive and high-throughput tool for measuring cellular responses to osmomechanical stimuli.

CaMPARI2-Based CRISPRi Screen Reveals Knowns and Novel Regulators of Osmomechanical Signaling

We next integrated CaMPARI2 with high-throughput pooled CRISPR interference (CRISPRi) screening—termed CaRPOOL (Calcium-Recording Pooled screening platform)—to systematically identify genes involved in osmomechanical signaling. To this end, we established a HEK293T cell line stably expressing both the CRISPRi machinery (dCas9-KRAB) [22]and CaMPARI2 and transduced it with a lentiviral sgRNA library targeting 2,418 membrane-associated genes (H6 library from CRISPRi-v2) [23]along with 250 non-targeting controls. We focused on membrane proteins because known mechanotransducers, such as ion channels and GPCRs, are predominantly membrane-localized.

Following selection and expansion, cells were exposed to hypotonic stimulation and 3 minutes of violet light to induce CaMPARI2 photoconversion. A portion of the population was retained as an input control, while the remainder was sorted by fluorescence-activated cell sorting (FACS) based on the CaMPARI2 red/green (R/G) ratio. Cells with low R/G ratios—indicative of reduced calcium responses—were isolated by FACS (bottom 15%). The representation of each sgRNA was quantified in both input and sorted populations by next-generation sequencing (NGS). Comparison of sgRNA abundance between populations enabled identification of genes important for osmomechanical sensing, whose sgRNAs would be enriched in the sorted low R/G population (Figure 2A, Table S2).

Our screen recovered several genes with known or plausible functions in mechanical signaling (Figure 2B), including *TMC1* and *USH2A*, which function in cochlear hair cells to mediate auditory mechanotransduction—TMC1 as a pore-forming component of the mechanosensory channel [24, 25] and USH2A as a structural element stabilizing stereocilia bundles[26]. We also identified *ITGA7* [27, 28] and *LARGE1*[29], which facilitate and maintain cell-matrix adhesion essential for force transmission; *ADGRG6*, *ADGRE2*, and *ANTXR1*, adhesion GPCRs that sense extracellular matrix stiffness or tension to activate downstream signaling[30]; *RIPOR1*, which regulates actin cytoskeleton dynamics in response to mechanical cues[31]; and *GJB6* and *GJC1*, gap junction proteins that coordinate intercellular communication during mechanically induced responses[32, 33]. These results validated the reliability of our screening approach.

We also identified genes not previously linked to osmomechanosensing and selected three top hits showing consistent phenotypes across two screen replicates for validation: *CCR7*, *GALNT3*, and *GAL3ST4*. *CCR7* encodes a chemokine receptor[34], while GALNT3 and GAL3ST4 are involved in glycosylation pathways[35, 36]. We cloned sgRNAs for each gene and individually validated their phenotypes by calcium imaging using GCaMP8f, orthogonal to our screening approach. Knockdown of each gene (Figure S2A) resulted in reduced HEK293T cell responses to hypotonic stimulation, albeit to varying degrees (Figures 2D and S2B), confirming the reliability of the screen.

Knockdown of *CCR7* resulted in the most significant reduction in cellular response to hypotonic stimulation (Figure 2D). Conversely, ectopic overexpression of *CCR7* markedly enhanced calcium responses to hypotonic stimulation, as measured by GCaMP8f fluorescence (Figure 2E). Notably, overexpression of *CCR6*, a closely related chemokine receptor, did not increase osmomechanical calcium signaling (Figure S2C), indicating a specific role for CCR7 in this process.

In summary, our results highlight the CaMPARI2-based CRISPRi screen as an effective

and scalable platform for discovering regulators of calcium responses to environmental stimuli and uncover *CCR7* as a novel modulator of osmomechanical signal transduction.

CCR7 Regulates Osmomechanical Calcium Signaling Through PIEZO1-Mediated Calcium Influx

We next investigated the mechanism by which CCR7 regulates osmomechanical calcium signaling. As a GPCR, CCR7 may modulate cytosolic calcium levels through two principal pathways: (1) the Gαq-PLCβ-IP_3/DAG signaling cascade, in which inositol 1,4,5-trisphosphate (IP_3) binds to IP_3 receptor type 3 (ITPR3) on the endoplasmic reticulum (ER), triggering calcium release from ER stores into the cytosol[37], or (2) modulation of plasma membrane ion channels via G-protein coupling, leading to extracellular calcium influx[38, 39].

To determine whether hypotonic stimulation mobilizes ER calcium stores, we knocked down *ITPR3*, which encodes the IP_3 receptor responsible for ER calcium release (Figure S3A). GCaMP8f calcium imaging revealed that *ITPR3* knockdown did not affect HEK293T cell responses to hypotonic stimulation (Figure 3A), indicating that ER calcium stores do not contribute significantly to the osmomechanical response. In contrast, removal of extracellular calcium using calcium-free buffer dramatically reduced the hypotonic-induced calcium response (Figure 3B). These results demonstrate that the calcium increase induced by hypotonic mechanical stimulation in HEK293T cells primarily results from extracellular calcium influx.

PIEZO1 is a mechanosensitive cation channel responsible for Ca^{2+} influx in diverse mechanical responses across multiple cell types[40-44]. We therefore examined whether PIEZO1 mediates calcium influx under osmomechanical stimulation. Knockdown of *PIEZO1* in HEK293T cells significantly reduced the hypotonic calcium response, as determined by both GCaMP8f imaging and CaMPARI2 assays (Figures 3C-D and S3B), indicating a major role for PIEZO1 in mediating the HEK293T hypotonic response.

We next investigated whether CCR7 influences the hypotonic response through PIEZO1. We overexpressed *CCR7* in *PIEZO1*-knockdown HEK293T cells and performed GCaMP8f calcium imaging. In *PIEZO1*-knockdown cells, *CCR7* overexpression no longer enhanced the hypotonic response (Figure 3E), suggesting that CCR7's effect is PIEZO1-dependent. To exclude potential residual PIEZO1 activity in knockdown cells, we generated a *PIEZO1* knockout HEK293T cell line. These cells exhibited near-complete loss of calcium response to hypotonic treatment (Figure S3C). Consistently, CCR7 overexpression failed to enhance the hypotonic response in *PIEZO1*-KO cells (Figure S3C), confirming that CCR7 modulates the HEK293T hypotonic response in a PIEZO1-dependent manner.

Together, these findings indicate that CCR7 regulates cellular responses to osmomechanical stimuli through PIEZO1-mediated extracellular calcium influx.

CCR7 Modulates Osmomechanical Calcium Signaling via the Gαs-cAMP-PKA Pathway

A recent study reported that protein kinase A (PKA) directly phosphorylates PIEZO1 to enhance its mechanosensitivity[45, 46]. Because PKA can be activated downstream of GPCR signaling through the Gαs-cAMP pathway, we examined whether CCR7 modulates PIEZO1 signaling via this mechanism.

Knockdown of Gαs (encoded by *GNAS*) using CRISPRi in HEK293T cells markedly reduced the calcium response to hypotonic stimulation and almost completely abolished the enhancement induced by CCR7 overexpression (Figures 4A and S4A), indicating that CCR7 acts through Gαs-dependent signaling.

Because Gαs activates adenylate cyclase (AC) to produce cyclic adenosine monophosphate (cAMP), we next tested whether hypotonic stimulation elevates intracellular cAMP levels in HEK293T cells. Using the GloSensor™ cAMP assay, we observed a sustained increase in cAMP following hypotonic stimulation, whereas

isotonic treatment showed little change (Figure 4B). Forskolin, an AC activator, served as a positive control (Figure S4B). Consistent results were obtained using the genetically encoded cAMP sensor GFlamp2[47, 48], which showed osmolarity-dependent increases in cAMP (Figure S4C), confirming AC activation.

Furthermore, knocking down *ADCY3*, a major AC isoform expressed in HEK293T cells, substantially reduced the hypotonic calcium response and prevented CCR7 from enhancing it (Figures 4C and S4D). Similarly, inhibiting AC activity with the small-molecule inhibitor SQ22536 significantly diminished the calcium response (Figure 4D).

Since cAMP activates PKA, we next asked whether PKA mediates CCR7's effect. Inhibition of PKA, either by silencing *PRKACA* (encoding the PKA catalytic subunit) or by treatment with H-89, strongly reduced calcium responses to hypotonic stimulation (Figures 4E-F and S4E). *PRKACA* knockdown also eliminated the potentiating effect of CCR7 overexpression (Figure 4E). Thus, PKA activity is required for CCR7-dependent enhancement of osmomechanical calcium influx.

Together, these findings reveal that CCR7 enhances osmomechanical calcium Signaling through the Gαs-AC-cAMP-PKA signaling axis (Figure 4G).

CCR7 Expression is Induced by Osmomechanical Stimulation and Enhances Calcium Signaling in Immune Cells

CCR7 is highly expressed in immune cells, including T cells and dendritic cells (DCs), where it regulates migration and activation during immune responses[49-52]. Because these cells encounter variable mechanical environments during circulation and tissue infiltration, we asked whether they respond to osmomechanical cues and whether CCR7 participates in this process.

We first sought to determine how immune cells respond to osmomechanical stimulation at the transcriptomic level. To this end, we treated Jurkat T cells with hypotonic or

isotonic medium for 6 hours and performed RNA-sequencing (Figure 5A). Hypotonic stimulation induced widespread transcriptional changes, with 932 genes upregulated and 539 downregulated (Figure 5B). Gene ontology analysis revealed enrichment of pathways related to T cell activation, lymphocyte differentiation, and Wnt signaling (Figures 5C and 5D), indicating that osmomechanical stress activates transcriptional programs associated with T cell functional regulation.

Among the upregulated genes, *CCR7* expression was significantly increased under hypotonic conditions (Figure 5B). Quantitative PCR confirmed elevated *CCR7 mRNA* levels after hypotonic treatment, showing progressive induction from 4 to 6 hours (Figure 5E), consistent with previous observations that mechanical confinement upregulates *CCR7* in immune cells[49]. These findings suggest that osmomechanical cues induce *CCR7* expression as part of a mechanoadaptive transcriptional response.

We next examined whether increased *CCR7* expression enhances the cellular response to hypotonic stress. Overexpression of CCR7 significantly augmented calcium influx upon hypotonic stimulation in Jurkat T cells, as measured by Fluo-4 calcium imaging (Figure 5F).

Together, these results show that osmomechanical stimuli upregulate *CCR7* expression in immune cells, and elevated CCR7 levels amplify calcium responses to hypotonic stress. This suggests the existence of a positive feedback mechanism in which osmomechanical activation enhances *CCR7* expression, which in turn sensitizes cells to subsequent mechanical cues, thereby facilitating rapid immunomechanical adaptation.

Discussion

This study establishes CaRPOOL, a FACS-based pooled screening system as a scalable platform for dissecting cellular responses to environmental stimuli. By integrating a calcium-sensitive photoconvertible reporter CaMPARI2 with CRISPR interference and flow cytometry, we converted transient calcium dynamics into a stable fluorescence

ratio measurable across large populations. This approach overcomes a key limitation of traditional imaging-based calcium assays, enabling pooled, high-throughput genetic analysis of dynamic signaling events.

We applied this technology to osmotic mechanical stimulation as a proof-of-concept. Changes in extracellular osmolarity deform cell membranes and generate mechanical stress in a controllable manner. HEK293T cells displayed stimulus-dependent calcium responses to both hypertonic and hypotonic conditions, which CaMPARI2 captured as quantifiable fluorescence conversions. These results validated the assay's sensitivity and demonstrated osmotic stress as an effective model for large-scale screening of mechanotransduction.

Using a CRISPRi library targeting membrane-associated genes, the system identified several known mechanosensory components and uncovered CCR7 as a previously unrecognized regulator of osmomechanical calcium signaling. Mechanistic analyses showed that upon hypotonic activation, CCR7 engages Gαs to activate adenylate cyclase and increase cAMP, leading to PKA activation, which enhances PIEZO1 channel activity and calcium influx. The pathway parallels other GPCR-mediated mechanosensory mechanisms, such as the AT1R-TRPC axis[53, 54] , PIEZO1-CALCRL / RAMP2 axis [46]and reveals direct crosstalk between chemokine receptor signaling and mechanically gated ion channels.

Although ion channels have been traditionally viewed as primary mechanosensors, accumulating evidence indicates that GPCRs can also respond to physical forces. GPR68[14], AT1R[55, 56], $GABA_B$[57], and several adhesion GPCRs[58-60] exemplify mechanically activated receptors that couple extracellular deformation to intracellular calcium signaling. CCR7 adds to this repertoire and highlights that mechanical stimuli can activate immune receptors even independent of their canonical ligands. Indeed, we observed that osmomechanical stress upregulated *CCR7* expression in Jurkat T cells, and that CCR7 overexpression enhanced calcium responses to hypotonic stimulation.

These findings suggest that CCR7 participates in a mechanoadaptive program where mechanical activation induces its own expression, thereby sensitizing cells to further mechanical cues.

The mechanosensitive properties of CCR7 are particularly relevant in the immune system, where migrating cells continually encounter shear stress, compression, and osmotic fluctuations[61, 62]. Such forces influence receptor signaling, activation thresholds, and effector functions. CCR7 is essential for lymphocyte homing and dendritic cell trafficking[63, 64]—processes that inherently involve mechanical challenge—and has been linked to mechanical modulation in both physiological and pathological contexts. The CCR7-Gαs-PKA-PIEZO1 axis described here may therefore represent a general mechanism by which immune cells translate physical changes in their environment into biochemical responses that fine-tune their function.

Beyond osmomechanical stimulation, the CaMPARI2 platform offers a broadly applicable framework for functional genomic screening of dynamic responses. Because calcium flux serves as a universal signaling output, this system can be adapted to probe diverse stimuli, including thermal and chemical perturbations. It is compatible with CRISPRa, CRISPR knockout, and genome-wide libraries, allowing cell-type-specific exploration of sensory transduction in epithelial, immune, neuronal or tumor models[65]. In cancer research, for example, mechanical cues from extracellular matrix stiffening and tissue compression drive invasion and therapy resistance; screening for mechanosensitive regulators may reveal new therapeutic targets.

In conclusion, our CaMPARI2-based system provides a versatile and unbiased method to capture transient calcium signals and link them to genetic determinants of cellular response. Applied to osmotic stress, it uncovered CCR7 as a mechanosensitive GPCR that modulates PIEZO1-mediated calcium influx through the Gαs-cAMP-PKA pathway. Together, these results validate the power of this technological approach and highlight

its potential for large-scale mapping of signaling networks that couple mechanical and chemical cues to cell behavior.

MATERIALS AND METHODS

Cell culture

All cells were maintained at 37 °C in a humidified incubator with 5% CO_2. HEK293T cells (ATCC) were cultured in Dulbecco's Modified Eagle Medium (DMEM; Gibco, C11995500BT) supplemented with 10% fetal bovine serum (FBS; TransGen Biotech, FS301-02) and 1% penicillin-streptomycin (Aladdin, P301861). Jurkat cells were maintained in RPMI 1640 medium (Gibco, 11875093) with the same supplements. PIEZO1-knockout HEK293T cells were generously provided by Dr. Yan (Shenzhen Bay Laboratory). All cell lines were mycoplasma negative detected by MycAwayTM Plus-Color One-Step Mycoplasma Detec- tion Kit (Yeasen, 40612ES25).

sgRNA cloning.

Individual sgRNAs were cloned into the pLG15 vector using BstXI and Bpu1102I restriction sites as previously described (PMID:).The pLG15 vector contains a mouse U6 promoter for sgRNA expression and an EF-1α promoter driving puromycin resistance and BFP for selection. sgRNA sequences are provided in Table S3.

Lentivirus production for the sgRNA library

HEK293T cells were seeded in 15 cm dishes and incubated for 24 h before transfection. For each dish, 4 μg of sgRNA library plasmid and 12 μg of third-generation packaging plasmid mix (1:1:1 ratio of pMDLg/pRRE (Addgene 12251), pRSV-Rev (Addgene 12253), and pMD2.G (Addgene 12259)) were diluted in 3 mL of Opti-MEM (Gibco, 31986-07). Polyethylenimine (PEI, 2 mg/mL; Yeasen, 40816ES03) was added at 36 μL per reaction, mixed thoroughly by vortexing, and incubated for 15-20 min at room temperature before being added to the cells. Viral supernatants were harvested 48 h post-transfection, filtered through 0.45 μm filters (Millipore SLHV033RB), and used immediately or stored at −80 °C.

Quantitative real-time PCR (qPCR)

Total RNA was extracted using the MolPure® Cell RNA Kit (Yeasen, 19231ES50).

418 cDNA was synthesized from extracted RNA using the TransScript® One-Step gDNA
419 Removal and cDNA Synthesis SuperMix (TransGen, AT311-03). qPCR was performed
420 with AceQ qPCR SYBR Green Master Mix (Vazyme, CQ111-02) on an FDQ-96A
421 fluorescence quantitative PCR system following manufacturer instructions. Gene
422 expression was normalized to GAPDH.
423
424 **Hypotonic and hypertonic treatments**
425 For flow-cytometry-based CaMPARI2 measurements, isotonic conditions consisted of
426 DMEM. Hypotonic medium was prepared by diluting DMEM with an equal volume of
427 double-distilled water (ddH_2O), while hypertonic medium was made by supplementing
428 DMEM with 400 mM sorbitol.
429
430 For calcium imaging and microplate reader assays, the isotonic buffer
431 contained130 mM NaCl, 3 mM KCl, 2.5 mM $CaCl_2$, 0.6 mM $MgCl_2$, 10 mM HEPES,
432 and 10 mM glucose, adjusted to pH 7.4 with NaOH in ddH_2O. Hypotonic buffer was
433 prepared by diluting the isotonic buffer 1:1 (v/v) with ddH_2O, and hypertonic buffer was
434 produced by adding 400 mM sorbitol to the isotonic buffer. The calcium-free buffer
435 contained 130 mM NaCl, 3 mM KCl, 0.6 mM $MgCl_2$, 10 mM HEPES, and 10 mM
436 glucose, adjusted to pH 7.4 with NaOH in ddH_2O, without $CaCl_2$.
437
438 For experiments using defined sorbitol-based osmotic solutions containing only
439 sorbitol, water, and $CaCl_2$, the hypertonic solution (~700 mOsm) consisted of
440 693 mM sorbitol and 2.5 mM $CaCl_2$ in ddH_2O; the isotonic solution (~300 mOsm)
441 contained 293 mM sorbitol and 2.5 mM $CaCl_2$ in ddH_2O; and the hypotonic solution
442 (~150 mOsm) included 143 mM sorbitol and 2.5 mM $CaCl_2$ in ddH_2O.
443
444 **Drug treatments**
445 For adenylyl cyclase or protein kinase A inhibition, cells were seeded and incubated
446 overnight, then treated with SQ22536 (100 μM; MCE, HY-100396) or
447 H-89 (10 μM; MCE, HY-15979) for 2 h prior to experiments.

For adenylyl cyclase activation, cells were treated with forskolin (20 μM; SelleckChem, S2449) for 5 s immediately before stimulation.

Measurement of the intracellular calcium concentration by fluorescence imaging

HEK293T cells were loaded with Fluo-4 AM or transfected with GCaMP8f. Prior to imaging, the culture medium was replaced with pre-warmed isotonic solution or the indicated test solutions.

Calcium fluorescence images were acquired over 10 min at room temperature using a Nikon Ti2-U fluorescence microscope (Japan) equipped with a 20× objective and a 488 nm excitation filter. In parallel, population-level fluorescence signals were measured using a microplate reader (excitation 488 nm, emission 525 nm). The experimental protocol consisted of a 2 min baseline recording in isotonic solution, followed by exposure to hypertonic or hypotonic solution for 1-2 min, and recovery in isotonic solution for an additional 6 min.

For single-cell calcium flux analysis, individual cells were outlined as regions of interest (ROI), and fluorescence intensity was quantified over time. Changes in intracellular calcium were expressed as $\Delta F/F_0 = (F_t / F_0) \times 100\%$, where F_t is fluorescence at time t and F_0 is the mean baseline fluorescence before osmotic stimulation. Statistical analyses were performed using GraphPad Prism (v9.0), calculating the mean $\Delta F/F_0$ from three consecutive time points around each peak calcium response.

Measurement of the intracellular calcium concentration by microplate reader

HEK293T cells were loaded with Fluo-4 AM or transfected with GCaMP8f and seeded into black-walled 96-well plates. Each well was filled with 100 μL isotonic solution. Fluorescence measurements were performed using a microplate reader under the following conditions: excitation at 488 nm, emission at 525 nm, at room temperature.

The recording protocol consisted of an initial 1 min baseline measurement in isotonic solution, followed by addition of hypertonic or hypotonic solution and continuous recording for an additional 9 min. Relative changes in fluorescence intensity were calculated as $\Delta F/F_0 = (F_t / F_0) \times 100\%$, identical to the imaging-based method. Statistical analyses were performed in GraphPad Prism, with significance assessed by comparing mean $\Delta F/F_0$ values derived from three time points around the peak calcium signal.

Measurement of the intracellular calcium concentration by CaMPARI2 using flow cytometry

HEK293T cells stably expressing CaMPARI2 were seeded into 24-well plates one day prior to experiments. Before measurement, cells were incubated in pre-warmed isotonic, hypotonic, or hypertonic solution and illuminated with a 405 nm violet LED for 3 min to induce CaMPARI2 photoconversion.

Following illumination, cells were trypsinized, collected, and analyzed by flow cytometry. Fluorescence signals were recorded in the GFP (488 nm excitation) and RFP (561 nm excitation) channels, and the RFP/GFP ratio was calculated to quantify the extent of CaMPARI2 photoconversion, reflecting calcium-dependent activation. Flow cytometry data were processed using FlowJo v10.7 (Tree Star).

CaRPOOL screen and data analysis.

HEK293T cells were stably integrated with CaMPARI2 via lentiviral transduction. Seven days after transduction, GFP-positive cells were sorted by fluorescence-activated cell sorting (FACS; BD FACSAria SORP) to isolate CaMPARI2-expressing populations.

Lentivirus carrying the membrane-protein sgRNA library was produced as described above and transduced into CaMPARI2-CRISPRi HEK293T cells at a multiplicity of

infection (MOI < 0.3). Forty-eight hours post-infection, cells were selected with puromycin (2 μg/mL) for 48 h to remove uninfected cells.

For pooled photoconversion screening, approximately 3×10^7 transduced cells were plated in 150 mm dishes and illuminated with 405 nm violet light for 3 min. A fraction of 5×10^6 cells was collected as the input control, while the remaining ~3×10^7 cells were subjected to FACS sorting to isolate the lowest 15% of cells based on the CaMPARI2 RFP/GFP (R/G) ratio, representing reduced calcium responses.

Genomic DNA was extracted from both input and sorted populations using DNAiso Reagent (Takara, 9770Q). sgRNA cassettes were PCR-amplified with 2× Phanta Flash Master Mix (Vazyme, P510-02) using primers oSeq_dual_p7 and oSeq_dual_p5 (sequences in Table S3) and purified using Hieff NGS DNA Selection Beads (Yeasen, 12601ES08). Libraries were sequenced on the DNBSEQ-T7 platform (MGI Tech).

Sequencing reads (FASTQ Read2) were trimmed and aligned to the reference sgRNA library using Bowtie v1.1.2 (Table S1). Guide and gene-level enrichment scores were computed using the MAGeCK-iNC pipeline [66, 67] to identify sgRNAs significantly associated with altered CaMPARI2 photoconversion phenotypes (Table S2).

Measurement of intracellular cAMP

Intracellular cyclic AMP (cAMP) levels were measured using either a luminescent biosensor (pGloSensor-22F) or a fluorescent biosensor (GFlamp2).

For luminescence-based assays, HEK293T cells were transfected with the pGloSensor-22F cAMP reporter plasmid and incubated for 48 h. Cells were then subjected to isosmotic or hypoosmotic stimulation at time 0 min and immediately placed in a microplate reader at room temperature. Luminescence intensity was monitored continuously for 10 min to track dynamic cAMP changes.

For fluorescence-based assays, HEK293T cells were transfected with the GFlamp2 cAMP reporter plasmid and seeded into 96-well black-walled plates. Each well contained 100 μL isotonic solution prior to recording. Fluorescence signals (excitation 405 nm, emission 510 nm) were measured using a microplate reader under standard conditions. Cells were recorded for 1 min under isotonic conditions, followed by an additional 19 min recording after replacement with isotonic or hypotonic solution. cAMP dynamics were quantified from real-time fluorescence traces using GraphPad Prism (v9.0).

RNA-seq and data analysis

Jurkat cells were collected after treatment, and total RNA was extracted using TRIzol Reagent (Ambion). RNA concentration and purity were measured using a Qubit 4.0 Fluorometer (Thermo Scientific), and RNA integrity was evaluated using an Agilent 2100 Bioanalyzer (Agilent Technologies). Sequencing libraries were generated using the Hieff NGS® Ultima Dual-Mode mRNA Library Prep Kit for Illumina® (Yeasen, Cat. No. 12301), following the manufacturer's instructions. High-throughput sequencing was performed on the DNBSEQ-T7 platform (Geneplus-Shenzhen), producing at least 12 Gb of 150 bp paired-end (PE150) reads per sample.

Raw sequencing reads were aligned to the human reference genome (GRCh38) using STAR (v2.7.6a), and gene-level expression was quantified with StringTie2 (v2.0.4). Expression normalization was performed using both Fragments Per Kilobase of transcript per Million mapped reads (FPKM) and Transcripts Per Million (TPM) methods.

Differential gene expression between experimental conditions was analyzed using the DESeq2 R package v1.26.0. P-values were adjusted for multiple testing via the Benjamini-Hochberg correction method, and genes with adjusted $P < 0.05$ and $|\log_2(\text{fold change})| \geq 1$ were considered significantly differentially expressed.

Gene Ontology (GO) enrichment analysis of the differentially expressed genes was performed using GSEAPY (v1.1.3).

Statistical Analysis

All statistical analyses were performed using GraphPad Prism v9.0 (GraphPad Software). For comparisons between two independent groups, unpaired two-tailed Student's t-tests were applied when data met the assumptions of normality and homogeneity of variance. For non-parametric data, the Mann-Whitney U test was used. Comparisons involving more than two groups were analyzed using one-way ANOVA followed by appropriate post hoc tests. Data are presented as mean ± SEM (or mean ± SD where indicated), and statistical significance was defined as $P < 0.05$. Detailed statistical information, including sample sizes (n), specific tests applied, and exact P-values, are provided in the corresponding figure legends.

ACKNOWLEDGMENTS

We thank Dr. Zhiqiang Yan (Chinese Institutes for Medical Research) and Dr. Yang Xu (Southern University of Science and Technology) for generously providing reagents and offering valuable discussions on this project. We thank Xiaojia Wang for assistance on the project. We also thank the assistance of SUSTech Core Research Facilities on flow cytometry and imaging. This work was supported by the National Key Research and Development Program of China (2024YFA0919800), Shenzhen Medical Research Fund (A2303039), Guangdong Basic and Applied Basic Research Foundation (2023B151502007), National Natural Science Foundation of China (82171416) and Shenzhen Fundamental Research Program (JCYJ20220530112602006 and RCYX20221008092845052).

AUTHOR CONTRIBUTIONS

R.T. conceived and designed the study. M.O. and J.W. performed all experiments and data analyses under the guidance of R.T. M.O. and R.T. wrote the manuscript.

DECLARATION OF INTERESTS

The authors declare no competing interests.

SUPPLEMENTAL INFORMATION

Table S1: Raw sgRNA counts of the CaRPOOL screen

Table S2: MAGeCK-iNC results of the CaRPOOL screen

Table S3: sgRNA and primer sequences used in this study.

References

[1] GALLUZZI L, YAMAZAKI T, KROEMER G. Linking cellular stress responses to systemic homeostasis[J]. Nat Rev Mol Cell Biol, 2018, 19(11): 731-745.

[2] OCHOA C D, WU R F, TERADA L S. ROS signaling and ER stress in cardiovascular disease[J]. Mol Aspects Med, 2018, 63: 18-29.

[3] ZHANG W, WU Y, S J G. Membrane adhesion junctions regulate airway smooth muscle phenotype and function[J]. Physiol Rev, 2023, 103(3): 2321-2347.

[4] KEFAUVER J M, WARD A B, PATAPOUTIAN A. Discoveries in structure and physiology of mechanically activated ion channels[J]. Nature, 2020, 587(7835): 567-576.

[5] SCHOLZ N, DAHSE A K, KEMKEMER M, et al. Molecular sensing of mechano- and ligand-dependent adhesion GPCR dissociation[J]. Nature, 2023, 615(7954): 945-953.

[6] CATERINA M J, SCHUMACHER M A, TOMINAGA M, et al. The capsaicin receptor: a heat-activated ion channel in the pain pathway[J]. Nature, 1997, 389(6653): 816-824.

[7] VRIENS J, NILIUS B, VOETS T. Peripheral thermosensation in mammals[J]. Nat Rev Neurosci, 2014, 15(9): 573-589.

[8] SHI Y, HU J, XUE T. Light, opsins, and life: Mammalian photophysiological functions beyond image perception[J]. Neuron, 2025, 113(19): 3108-3128.

[9] BILLESBOLLE C B, DE MARCH C A, VAN DER VELDEN W J C, et al. Structural basis of odorant recognition by a human odorant receptor[J]. Nature, 2023, 615(7953): 742-749.

[10] DELVENTHAL R, CARLSON J R. Bitter taste receptors confer diverse functions to neurons[J]. Elife, 2016, 5

[11] RANADE S S, SYEDA R, PATAPOUTIAN A. Mechanically Activated Ion Channels[J]. Neuron, 2015, 87(6): 1162-1179.

[12] COSTE B, MATHUR J, SCHMIDT M, et al. Piezo1 and Piezo2 are essential components of distinct mechanically activated cation channels[J]. Science, 2010, 330(6000): 55-60.

[13] GONG J, LIU J, RONAN E A, et al. A Cold-Sensing Receptor Encoded by a Glutamate Receptor Gene[J]. Cell, 2019, 178(6): 1375-1386 e1311.

[14] XU J, MATHUR J, VESSIERES E, et al. GPR68 Senses Flow and Is Essential for Vascular Physiology[J]. Cell, 2018, 173(3): 762-775 e716.

[15] ZHANG Y, ROZSA M, LIANG Y, et al. Fast and sensitive GCaMP calcium indicators for imaging neural populations[J]. Nature, 2023, 615(7954): 884-891.

[16] FOSQUE B F, SUN Y, DANA H, et al. Neural circuits. Labeling of active neural circuits in vivo with designed calcium integrators[J]. Science, 2015, 347(6223): 755-760.

[17] MOEYAERT B, HOLT G, MADANGOPAL R, et al. Improved methods for marking active neuron populations[J]. Nat Commun, 2018, 9(1): 4440.

[18] YUAN F, YANG H, XUE Y, et al. OSCA1 mediates osmotic-stress-evoked Ca2+ increases vital for osmosensing in Arabidopsis[J]. Nature, 2014, 514(7522): 367-371.

[19] CENTEIO R, OUSINGSAWAT J, SCHREIBER R, et al. Ca(2+) Dependence of Volume-Regulated VRAC/LRRC8 and TMEM16A Cl(-) Channels[J]. Front Cell Dev Biol, 2020, 8: 596879.

[20] INOUE R, JENSEN L J, JIAN Z, et al. Synergistic activation of vascular TRPC6 channel by receptor and mechanical stimulation via phospholipase C/diacylglycerol and phospholipase A2/omega-hydroxylase/20-HETE pathways[J]. Circ Res, 2009, 104(12): 1399-1409.

[21] ZHANG M, WANG D, KANG Y, et al. Structure of the mechanosensitive OSCA channels[J]. Nat Struct Mol Biol, 2018, 25(9): 850-858.

[22] WEI T, LI J, LEI X, et al. Multimodal CRISPR screens uncover DDX39B as a global repressor of A-to-I RNA editing[J]. Cell Rep, 2025, 44(7): 116009.

[23] HORLBECK M A, GILBERT L A, VILLALTA J E, et al. Compact and highly active next-generation libraries for CRISPR-mediated gene repression and activation[J]. Elife, 2016, 5

[24] JEONG H, CLARK S, GOEHRING A, et al. Structures of the TMC-1 complex illuminate mechanosensory transduction[J]. Nature, 2022, 610(7933): 796-803.

[25] FU S, PAN X, LU M, et al. Human TMC1 and TMC2 are mechanically gated ion

channels[J]. Neuron, 2025, 113(3): 411-425 e414.
[26] GUAN Y, DU H B, YANG Z, et al. Deafness-Associated ADGRV1 Mutation Impairs USH2A Stability through Improper Phosphorylation of WHRN and WDSUB1 Recruitment[J]. Adv Sci (Weinh), 2023, 10(16): e2205993.
[27] LIGEZOWSKA A, BOYE K, EBLE J A, et al. Mechanically enforced bond dissociation reports synergistic influence of Mn2+ and Mg2+ on the interaction between integrin alpha7beta1 and invasin[J]. J Mol Recognit, 2011, 24(4): 715-723.
[28] DE REZENDE F F, MARTINS LIMA A, NILAND S, et al. Integrin alpha7beta1 is a redox-regulated target of hydrogen peroxide in vascular smooth muscle cell adhesion[J]. Free Radic Biol Med, 2012, 53(3): 521-531.
[29] BAO X, KOBAYASHI M, HATAKEYAMA S, et al. Tumor suppressor function of laminin-binding alpha-dystroglycan requires a distinct beta3-N-acetylglucosaminyltransferase[J]. Proc Natl Acad Sci U S A, 2009, 106(29): 12109-12114.
[30] HAMANN J, AUST G, ARAC D, et al. International Union of Basic and Clinical Pharmacology. XCIV. Adhesion G protein-coupled receptors[J]. Pharmacol Rev, 2015, 67(2): 338-367.
[31] LV Z, DING Y, CAO W, et al. Role of RHO family interacting cell polarization regulators (RIPORs) in health and disease: Recent advances and prospects[J]. Int J Biol Sci, 2022, 18(2): 800-808.
[32] ASMAR A, BARRETT-JOLLEY R, WERNER A, et al. Membrane channel gene expression in human costal and articular chondrocytes[J]. Organogenesis, 2016, 12(2): 94-107.
[33] LUKASHKINA V A, LEVIC S, LUKASHKIN A N, et al. A connexin30 mutation rescues hearing and reveals roles for gap junctions in cochlear amplification and micromechanics[J]. Nat Commun, 2017, 8: 14530.
[34] FORSTER R, DAVALOS-MISSLITZ A C, ROT A. CCR7 and its ligands: balancing immunity and tolerance[J]. Nat Rev Immunol, 2008, 8(5): 362-371.
[35] TOPAZ O, SHURMAN D L, BERGMAN R, et al. Mutations in GALNT3, encoding a protein involved in O-linked glycosylation, cause familial tumoral

calcinosis[J]. Nat Genet, 2004, 36(6): 579-581.
[36] SEKO A, HARA-KUGE S, YAMASHITA K. Molecular cloning and characterization of a novel human galactose 3-O-sulfotransferase that transfers sulfate to gal beta 1-->3galNAc residue in O-glycans[J]. J Biol Chem, 2001, 276(28): 25697-25704.
[37] LIANG C, ZHANG Q, CHEN X, et al. Human cancer cells generate spontaneous calcium transients and intercellular waves that modulate tumor growth[J]. Biomaterials, 2022, 290: 121823.
[38] ALBARRAN-JUAREZ J, IRING A, WANG S, et al. Piezo1 and G(q)/G(11) promote endothelial inflammation depending on flow pattern and integrin activation[J]. J Exp Med, 2018, 215(10): 2655-2672.
[39] ZHAO C, MACKINNON R. Structural and functional analyses of a GPCR-inhibited ion channel TRPM3[J]. Neuron, 2023, 111(1): 81-91 e87.
[40] CHOI D, PARK E, YU R P, et al. Piezo1-Regulated Mechanotransduction Controls Flow-Activated Lymphatic Expansion[J]. Circ Res, 2022, 131(2): e2-e21.
[41] ATCHA H, JAIRAMAN A, HOLT J R, et al. Mechanically activated ion channel Piezo1 modulates macrophage polarization and stiffness sensing[J]. Nat Commun, 2021, 12(1): 3256.
[42] JIANG F, YIN K, WU K, et al. The mechanosensitive Piezo1 channel mediates heart mechano-chemo transduction[J]. Nat Commun, 2021, 12(1): 869.
[43] SOLIS A G, BIELECKI P, STEACH H R, et al. Mechanosensation of cyclical force by PIEZO1 is essential for innate immunity[J]. Nature, 2019, 573(7772): 69-74.
[44] BARATCHI S, DANISH H, CHHEANG C, et al. Piezo1 expression in neutrophils regulates shear-induced NETosis[J]. Nat Commun, 2024, 15(1): 7023.
[45] ZHANG T, BI C, LI Y, et al. Phosphorylation of Piezo1 at a single residue, serine-1612, regulates its mechanosensitivity and in vivo mechanotransduction function[J]. Neuron, 2024, 112(21): 3618-3633 e3616.
[46] IRING A, JIN Y J, ALBARRAN-JUAREZ J, et al. Shear stress-induced endothelial adrenomedullin signaling regulates vascular tone and blood pressure[J]. J Clin Invest, 2019, 129(7): 2775-2791.

[47] LIU W, LIU C, REN P G, et al. An Improved Genetically Encoded Fluorescent cAMP Indicator for Sensitive cAMP Imaging and Fast Drug Screening[J]. Front Pharmacol, 2022, 13: 902290.

[48] WANG L, WU C, PENG W, et al. A high-performance genetically encoded fluorescent indicator for in vivo cAMP imaging[J]. Nat Commun, 2022, 13(1): 5363.

[49] ALRAIES Z, RIVERA C A, DELGADO M G, et al. Cell shape sensing licenses dendritic cells for homeostatic migration to lymph nodes[J]. Nat Immunol, 2024, 25(7): 1193-1206.

[50] CLATWORTHY M R, ARONIN C E, MATHEWS R J, et al. Immune complexes stimulate CCR7-dependent dendritic cell migration to lymph nodes[J]. Nat Med, 2014, 20(12): 1458-1463.

[51] LIU J, ZHANG X, CHEN K, et al. CCR7 Chemokine Receptor-Inducible lnc-Dpf3 Restrains Dendritic Cell Migration by Inhibiting HIF-1alpha-Mediated Glycolysis[J]. Immunity, 2019, 50(3): 600-615 e615.

[52] ALANKO J, UCAR M C, CANIGOVA N, et al. CCR7 acts as both a sensor and a sink for CCL19 to coordinate collective leukocyte migration[J]. Sci Immunol, 2023, 8(87): eadc9584.

[53] MEDEROS Y SCHNITZLER M, STORCH U, MEIBERS S, et al. Gq-coupled receptors as mechanosensors mediating myogenic vasoconstriction[J]. EMBO J, 2008, 27(23): 3092-3103.

[54] LIU C H, GONG Z, LIANG Z L, et al. Arrestin-biased AT1R agonism induces acute catecholamine secretion through TRPC3 coupling[J]. Nat Commun, 2017, 8: 14335.

[55] DURVASULA R V, PETERMANN A T, HIROMURA K, et al. Activation of a local tissue angiotensin system in podocytes by mechanical strain[J]. Kidney Int, 2004, 65(1): 30-39.

[56] KIJIMA K, MATSUBARA H, MURASAWA S, et al. Mechanical stretch induces enhanced expression of angiotensin II receptor subtypes in neonatal rat cardiac myocytes[J]. Circ Res, 1996, 79(4): 887-897.

[57] HUO Y, ZHOU Y, LIN L, et al. GABA-independent activation of GABA(B)

receptor by mechanical forces[J]. Nat Commun, 2025, 16(1): 9843.
[58] FU C, HUANG W, TANG Q, et al. Unveiling Mechanical Activation: GAIN Domain Unfolding and Dissociation in Adhesion GPCRs[J]. Nano Lett, 2023, 23(20): 9179-9186.
[59] MITGAU J, FRANKE J, SCHINNER C, et al. The N Terminus of Adhesion G Protein-Coupled Receptor GPR126/ADGRG6 as Allosteric Force Integrator[J]. Front Cell Dev Biol, 2022, 10: 873278.
[60] PETERSEN S C, LUO R, LIEBSCHER I, et al. The adhesion GPCR GPR126 has distinct, domain-dependent functions in Schwann cell development mediated by interaction with laminin-211[J]. Neuron, 2015, 85(4): 755-769.
[61] HUSE M. Mechanical forces in the immune system[J]. Nat Rev Immunol, 2017, 17(11): 679-690.
[62] ANGELI V, LIM H Y. Biomechanical control of lymphatic vessel physiology and functions[J]. Cell Mol Immunol, 2023, 20(9): 1051-1062.
[63] LIU J, ZHANG X, CHENG Y, et al. Dendritic cell migration in inflammation and immunity[J]. Cell Mol Immunol, 2021, 18(11): 2461-2471.
[64] KIERMAIER E, MOUSSION C, VELDKAMP C T, et al. Polysialylation controls dendritic cell trafficking by regulating chemokine recognition[J]. Science, 2016, 351(6269): 186-190.
[65] LI K, OUYANG M, ZHAN J, et al. CRISPR-based functional genomics screening in human-pluripotent-stem-cell-derived cell types[J]. Cell Genom, 2023, 3(5): 100300.
[66] TIAN R, GACHECHILADZE M A, LUDWIG C H, et al. CRISPR Interference-Based Platform for Multimodal Genetic Screens in Human iPSC-Derived Neurons[J]. Neuron, 2019, 104(2): 239-255 e212.
[67] TIAN R, ABARIENTOS A, HONG J, et al. Genome-wide CRISPRi/a screens in human neurons link lysosomal failure to ferroptosis[J]. Nat Neurosci, 2021, 24(7): 1020-1034.

785 **FIGURES AND FIGURE LEGENDS**

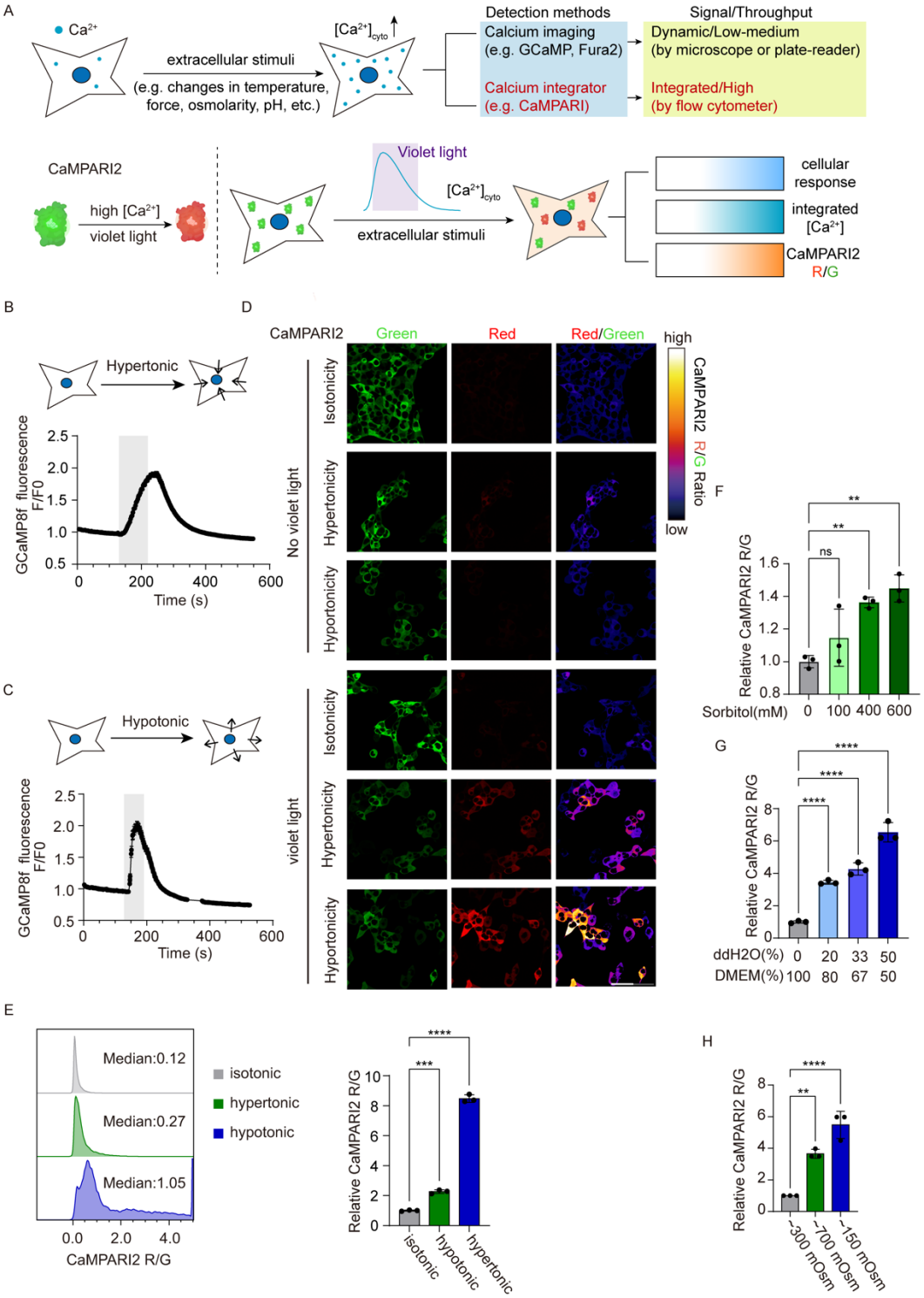

786

787 **Figure 1. CaMPARI2 enables high-throughput measurement of calcium responses**

788 **to osmotic mechanical stimulation**

(A) Schematic overview of calcium detection methods. Top: Dynamic sensors (e.g., GCaMP, Fura-2) enable real-time monitoring but are limited to low- or medium-throughput applications. Calcium integrators (e.g., CaMPARI) convert transient calcium signals into stable fluorescence outputs measurable by flow cytometry for high-throughput screening. Bottom: CaMPARI2 irreversibly switches from green to red fluorescence upon violet illumination in the presence of elevated [Ca^{2+}], with the red-to-green (R/G) ratio reflecting integrated calcium activity.

(B-C) Real-time calcium responses of HEK293T cells to (B) hypertonic (400 mM sorbitol in DMEM) or (C) hypotonic (1:1 DMEM:ddH_2O) stimulation monitored by GCaMP8f imaging. Gray shading indicates stimulation period. Traces show mean $\Delta F/F_0 \pm$ SEM. n = 79 cells (B), n = 126 cells (C).

(D) CaMPARI2 photoconversion in response to osmotic stimuli. Cells were exposed to isotonic (DMEM), hypotonic (1:1 DMEM:ddH_2O), or hypertonic (DMEM + 400 mM sorbitol) conditions during 3 min violet illumination (405 nm) or kept in dark (No violet). Representative images show green (unconverted, 488nm exitation), red (photoconverted, 561nm exitation), and red/green ratio. Scale bar, 40 μm.

(E) Flow cytometry quantification of CaMPARI2 R/G ratios. Left: Representative histograms. Right: Relative R/G ratios normalized to isotonic control. Data are mean ± SD (n = 3). ***$P < 0.001$, ****$P < 0.0001$; one-way ANOVA.

(F-G) Osmolarity-dependent CaMPARI2 responses measured by flow cytometry. Cells were exposed to indicated hypotonic (F) or hypertonic (G) treatments. Data are mean ± SD (n = 3). ns, not significant, *$p < 0.05$, **$p < 0.01$, ****$p < 0.0001$, One-way ANOVA.

(H) CaMPARI2 responses to defined osmotic solutions (sorbitol + water + $CaCl_2$). Cells were treated with hypertonic (~700 mOsm), isotonic (~300 mOsm), hypotonic (~150

mOsm), or ddH_2O during violet illumination. Relative R/G ratios normalized to ddH_2O are shown as mean ± SD (n = 3). **$p < 0.01$, ****$p < 0.0001$, One-way ANOVA.

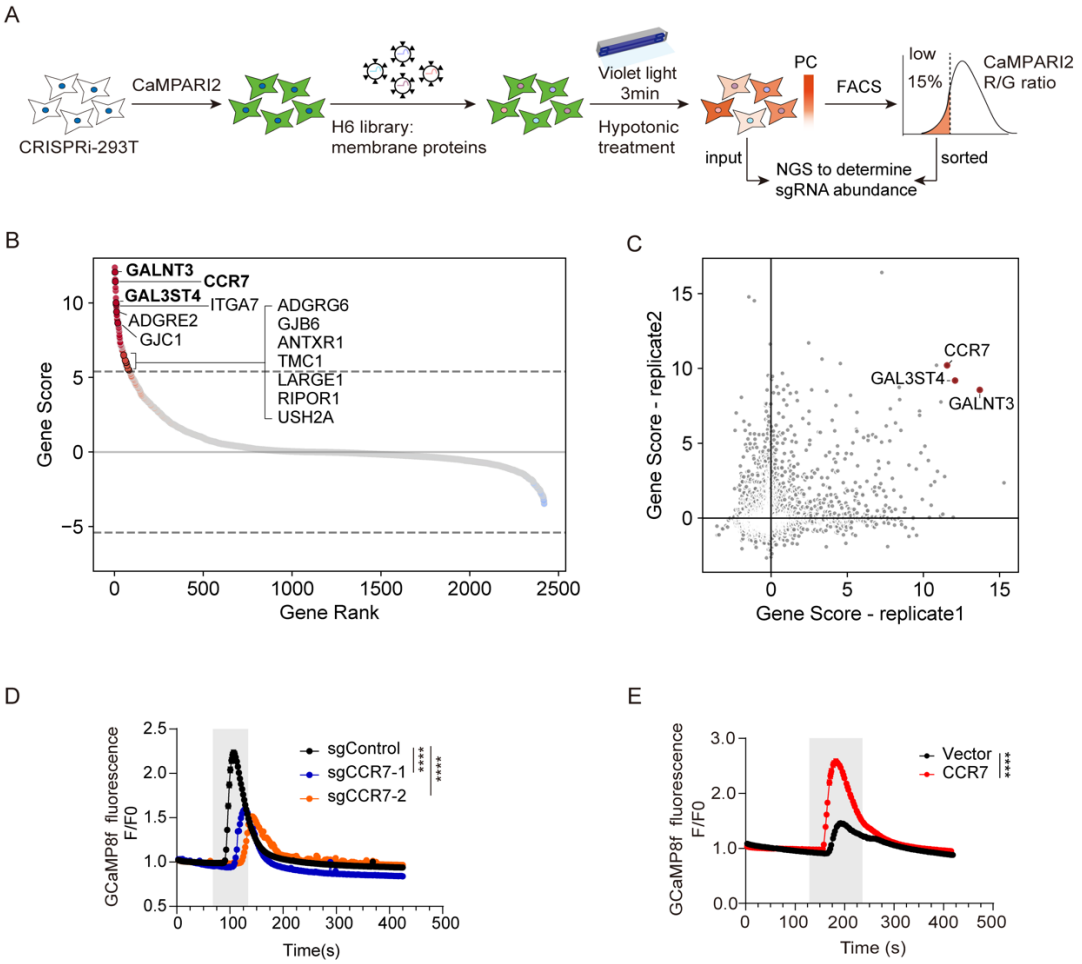

Figure 2. CaMPARI2-based CRISPRi screen reveals known and novel regulators of osmomechanical signaling

(A) Schematic of the CaMPARI2-based pooled CRISPRi screening workflow. HEK293T cells stably expressing CRISPRi machinery (dCas9-KRAB) and CaMPARI2 were transduced with a lentiviral sgRNA library targeting 2,418 membrane-associated genes (H6 library). Following selection and expansion, cells were subjected to hypotonic stimulation with 3 min violet light (405 nm) illumination to induce CaMPARI2 photoconversion. Cells with low CaMPARI2 R/G ratios (bottom 15%) were isolated by FACS, and sgRNA representation in input and sorted populations was quantified by next-generation sequencing (NGS) to identify genes regulating osmomechanical calcium responses.

(B) Gene-level scores from the CRISPRi screen. Genes are ranked by their scores from the MAGeCK-iNC pipeline. Genes with positive scores indicate enrichment of their sgRNAs in the low R/G population, and vice versa. Top hits include known mechanotransduction genes and novel candidates. Dashed horizontal lines indicate gene score threshold for FDR < 0.1.

(C) Comparison of gene scores from replicate 1 (x-axis) and replicate 2 (y-axis) shows reproducible hits, with representative candidates highlighted.

(D) Validation of screen hits by calcium imaging. HEK293T cells expressing two distinct sgRNAs targeting *CCR7* or sgControl were transduced with GCaMP8f and subjected to hypotonic stimulation. Traces show mean $\Delta F/F_0 \pm$ SEM (n = 409 cells for sgControl, n = 407 cells for sgCCR7-1, n = 424 cells for sgCCR7-2). Gray shading indicates stimulation period. ****P < 0.0001; One-way ANOVA.

(E) *CCR7* overexpression enhances calcium responses to hypotonic stimulation. HEK293T cells transfected with *CCR7,* or empty vector were subjected to hypotonic treatment, and GCaMP8f fluorescence was monitored. Traces show mean $\Delta F/F_0 \pm$ SEM (n = 177 cells for vector, n = 239 cells for *CCR7* overexpression). Gray shading indicates stimulation. ****P < 0.0001; unpaired two-tailed Student's t-test.

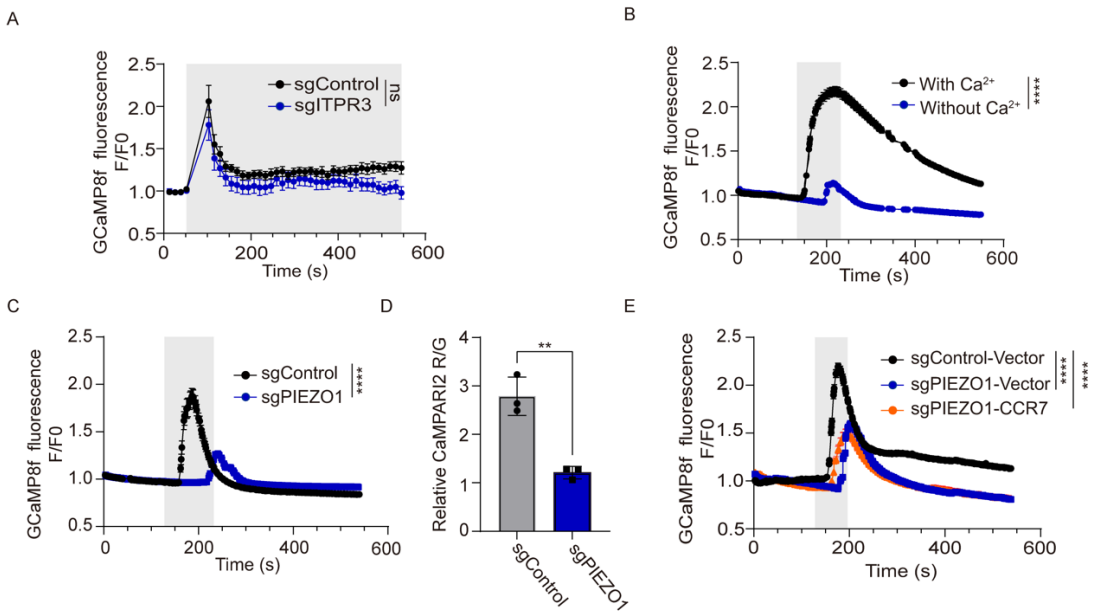

Figure 3. CCR7 modulates the response to hypoosmotic stimulation via PIEZO1

(A) Knockdown of IP_3 receptor 3 (*ITPR3*) does not affect the calcium response to hypotonic stimulation. GCaMP8f fluorescence traces of HEK293T cells expressing sgControl or sgITPR3 show similar calcium transients upon hypotonic treatment, measured by microplate reader. Traces represent mean $\Delta F/F_0 \pm$ SEM (n = 8). ns, not significant; unpaired two-tailed Student's t-test.

(B) Hypotonicity-induced calcium influx depends on extracellular Ca^{2+}. GCaMP8f fluorescence responses of HEK293T cells in isotonic buffer containing Ca^{2+} (130 mM NaCl + 2.5 mM $CaCl_2$) or in calcium-free buffer (no $CaCl_2$), measured by fluorescence imaging. Traces show mean $\Delta F/F_0 \pm$ SEM (n = 219 cells for with Ca^{2+} condition, n = 259 cells for without Ca^{2+} condition). Gray shading indicates stimulation period. ****$P < 0.0001$; unpaired two-tailed Student's t-test.

(C) *PIEZO1* knockdown abolishes hypotonicity-induced calcium responses. GCaMP8f fluorescence responses of HEK293T cells expressing sgControl or sgPIEZO1 exposed to hypotonic medium (1:1 DMEM:ddH_2O), measured by fluorescence imaging. Traces show mean $\Delta F/F_0 \pm$ SEM (n = 94 cells for sgControl, n = 299 cells for sgPIEZO1). ****$P < 0.0001$; unpaired two-tailed Student's t-test.

(D) CaMPARI2 assay confirms reduced calcium response in *PIEZO1*-depleted cells. Relative CaMPARI2 R/G ratios of sgPIEZO1 and sgControl cells after 3 min violet illumination during hypotonic stimulation. Data are mean ± SD (n = 3). **P < 0.01; unpaired two-tailed Student's t-test.

(E) *CCR7* overexpression fails to restore calcium influx in *PIEZO1*-knockdown cells. GCaMP8f traces of sgPIEZO1 cells transfected with vector or *CCR7* are shown alongside sgControl-Vector cells, measured by fluorescence imaging. Traces represent mean $\Delta F/F_0$ ± SEM (n = 312 cells for sgControl-Vector, n = 240 cells for sgPIEZO1-Vector, n = 196 cells for sgPIEZO1-CCR7). Gray shading indicates stimulation. ****P < 0.0001; one-way ANOVA.

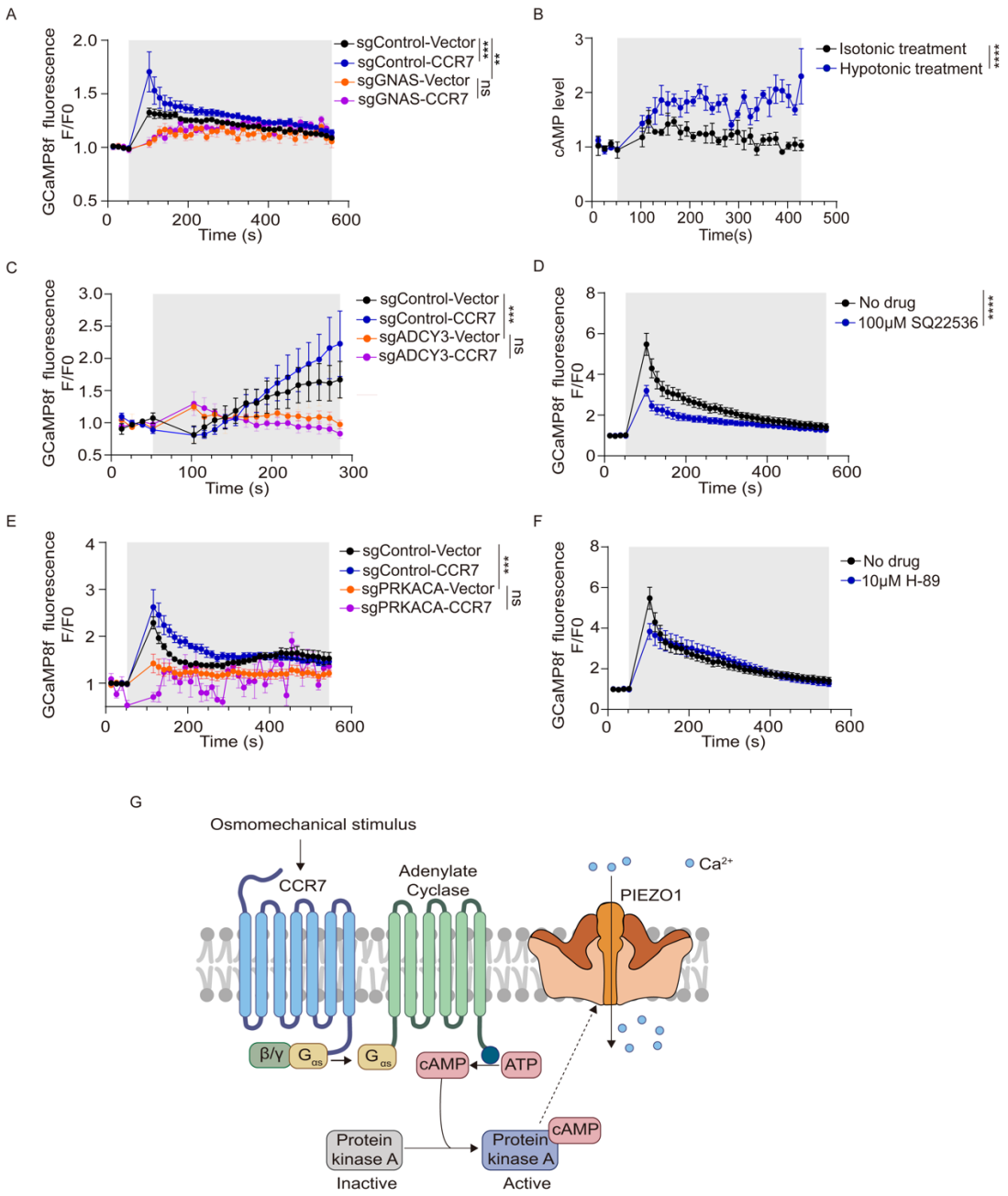

890

891

892 **Figure 4. CCR7 modulates PIEZO1-mediated calcium influx through the Gαs -**

893 **cAMP-PKA pathway**

894 (A) CCR7-mediated calcium response modulation requires Gαs signaling. HEK293T

895 cells expressing sgControl or sgGNAS with vector or *CCR7* were subjected to

896 hypotonic stimulation, measured by microplate reader. Traces show mean $\Delta F/F_0 \pm$ SEM

897 (n = 10). Gray shading indicates stimulation. ***P < 0.001, **P < 0.01, ns, not

898 significant; one-way ANOVA.

(B) Hypotonic stimulation increases intracellular cAMP levels. Cells expressing the cAMP biosensor pGloSensor-22F were monitored during isotonic or hypotonic treatment by microplate reader. Traces show mean cAMP levels ± SEM (n = 3). Gray shading indicates stimulation. ****P < 0.0001; Mann-Whitney U test.

(C) Adenylyl cyclase (*ADCY3*) knockdown abolishes CCR7-mediated enhancement of calcium responses. GCaMP8f traces of cells expressing sgControl or sgADCY3 with vector or CCR7, measured by microplate reader. Traces show mean $\Delta F/F_0$ ± SEM (n = 5). Gray shading indicates stimulation. ns, not significant, ***p < 0.001; one-way ANOVA.

(D) Adenylyl cyclase inhibitor SQ22536 blocks hypotonicity-induced calcium influx. HEK293T cells pretreated with 100 μM SQ22536 or vehicle were subjected to hypotonic stimulation, measured by microplate reader. Traces show mean $\Delta F/F_0$ ± SEM (n = 9). Gray shading indicates stimulation. ****P < 0.0001; Mann-Whitney U test.

(E) Protein kinase A catalytic subunit (*PRKACA*) knockdown reduces calcium responses to hypotonic stimulation and blocks CCR7-mediated enhancement of calcium responses. GCaMP8f traces of cells expressing sgControl or sgPRKACA with vector or *CCR7*, measured by microplate reader. Traces show mean $\Delta F/F_0$ ± SEM (n = 4). Gray shading indicates stimulation. *P<0.05, ***P < 0.001; one-way ANOVA.

(F) PKA inhibitor H-89 suppresses hypotonicity-induced calcium influx. HEK293T cells pretreated with 10 μM H-89 or vehicle were subjected to hypotonic treatment, measured by fluorescence imaging. Traces show mean $\Delta F/F_0$ ± SEM (n = 9). Gray shading indicates stimulation.

927 (G) Proposed model: Osmomechanical stimulation activates CCR7-Gαs-AC signaling,
928 producing cAMP that activates PKA to phosphorylate and enhance PIEZO1 activity,
929 leading to increased Ca^{2+} influx.
930

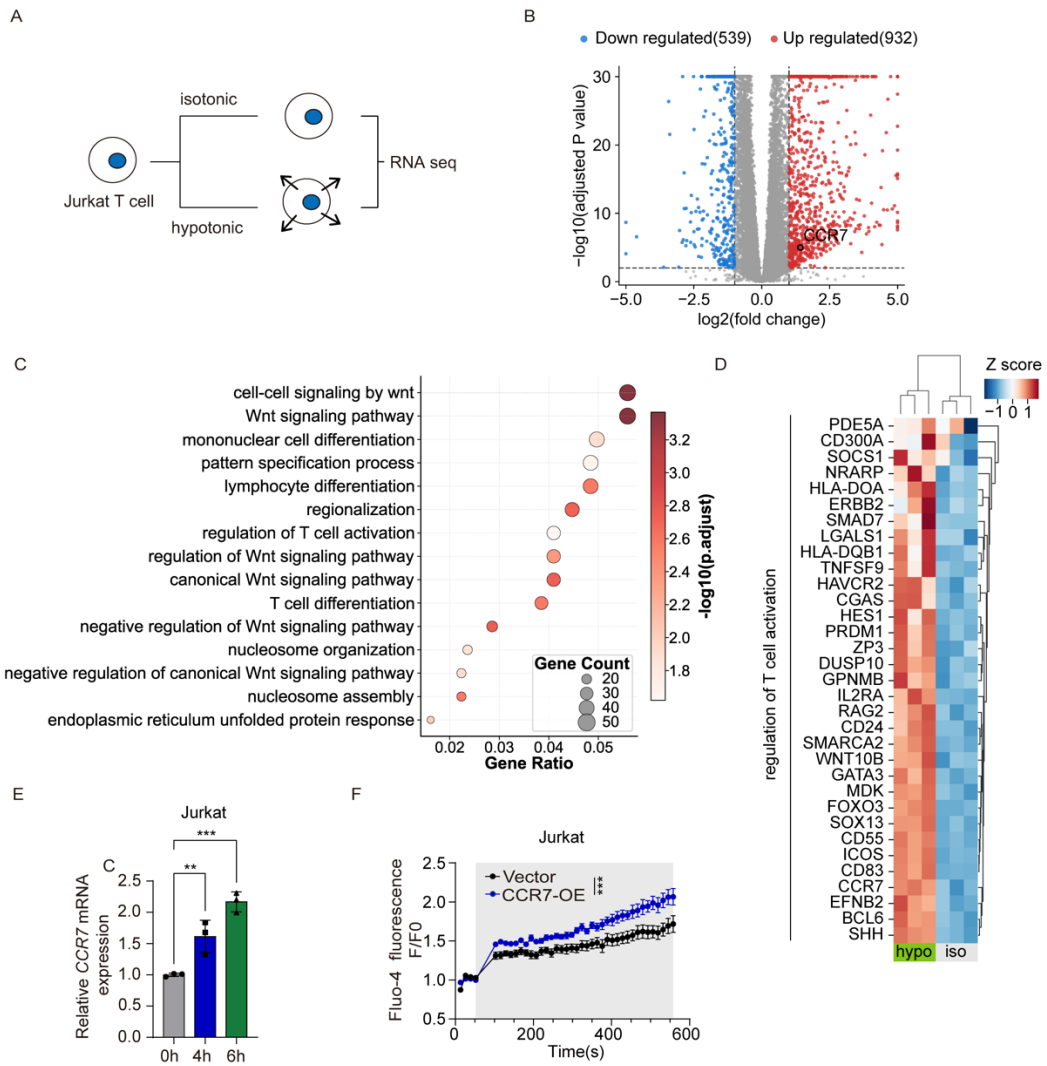

Figure 5. Hypotonic stimulation upregulates *CCR7* and enhances calcium responses in immune cells

(A) Schematic of RNA-seq experimental design. Jurkat T cells were exposed to isotonic or hypotonic medium for 6 hours, followed by RNA sequencing.

(B) Volcano plot showing differentially expressed genes in Jurkat T cells after hypotonic treatment. Blue dots represent downregulated genes (n = 539), red dots represent upregulated genes (n = 932), and gray dots represent genes with no significant change. *CCR7* is highlighted as significantly upregulated. Thresholds: |log2(fold change) | > 1 and adjusted P value < 0.05.

(C) Gene Ontology (GO) enrichment analysis of differentially expressed genes. Top 15 biological process terms ranked by adjusted P value are shown. Dot size represents gene count, and color intensity indicates −log10(adjusted P value).

(D) Heatmap showing expression of genes related to regulation of T cell activation. Z-score normalized expression levels in Jurkat cells under isotonic (iso) or hypotonic (hypo) conditions are displayed.

(E) Hypotonic stimulation upregulates *CCR7* mRNA expression in Jurkat cells. Relative *CCR7* mRNA levels at 0, 4, and 6 hours after hypotonic treatment, measured by qRT-PCR. Data are mean ± SD (n = 3). **P < 0.01, ***P < 0.001; one-way ANOVA.

(F) *CCR7* overexpression enhances calcium responses to hypotonic stimulation in Jurkat T cells. Fluo-4 fluorescence traces of cells transfected with empty vector or *CCR7*, measured by microplate reader. Traces show mean $\Delta F/F_0$ ± SEM (n = 8). Gray shading indicates stimulation. **P < 0.01; unpaired two-tailed Student's t-test.

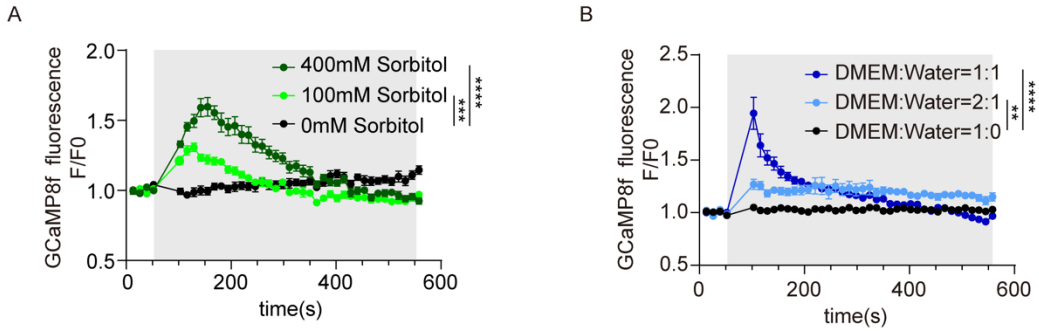

Figure S1. Calcium responses of HEK293T cells to hypotonic and hypertonic treatments

(A-B) Calcium responses of HEK293T cells to (A) hypertonic (100 mM and 400 mM sorbitol in DMEM) or (B) hypotonic (2:1 and 1:1 DMEM:ddH_2O) stimulation monitored by microplate reader using GCaMP8f. Traces show mean $\Delta F/F_0 \pm$ SEM (n = 10). Gray shading indicates stimulation. **$p < 0.01$, ***$p < 0.001$, ****$p < 0.0001$, One-way ANOVA.

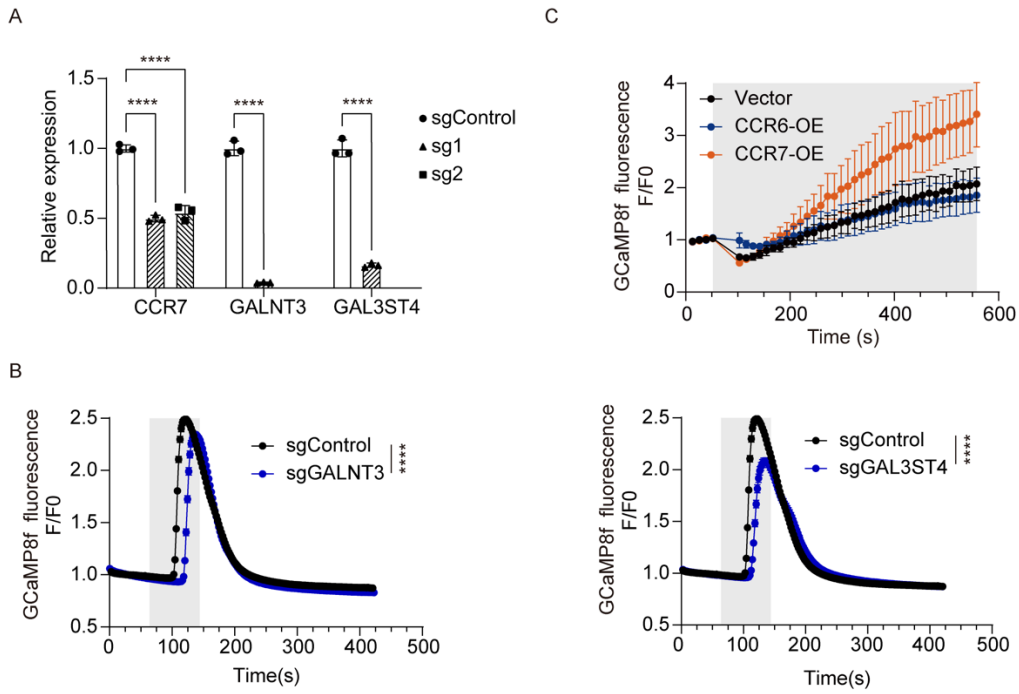

Figure S2. Validation of top hits from the CaMPARI2-based CRISPRi screen reveals *CCR7* as a key regulator of osmomechanical signaling

(A) Validation of CRISPRi-mediated gene knockdown. Relative mRNA expression levels of *CCR7*, *GALNT3*, and *GAL3ST4* in HEK293T cells expressing sgControl or gene-targeting sgRNAs were measured by qRT-PCR. Data are mean ± SEM (n = 3). ****P < 0.0001; unpaired two-tailed Student's t-test.

(B) Knockdown of *GAL3ST4* or *GALNT3* reduces calcium responses to hypotonic stimulation. GCaMP8f fluorescence traces of HEK293T cells expressing sgControl or sgGAL3ST4 (left) and sgControl or sgGALNT3 (right), measured by fluorescence imaging. Traces show mean $\Delta F/F_0 \pm$ SEM (n = 297 for sgControl, n = 196 for sgGAL3ST4, n = 312 sgGALNT3). Gray shading indicates stimulation. ****P < 0.0001; unpaired two-tailed Student's t-test.

(C) CCR7, but not CCR6, enhances osmomechanical calcium signaling. GCaMP8f fluorescence traces of HEK293T cells expressing empty vector, *CCR6*, or *CCR7* were

986 measured by microplate reader. Traces show mean $\Delta F/F_0 \pm$ SEM ($n = 5$). Gray shading
987 indicates stimulation.
988

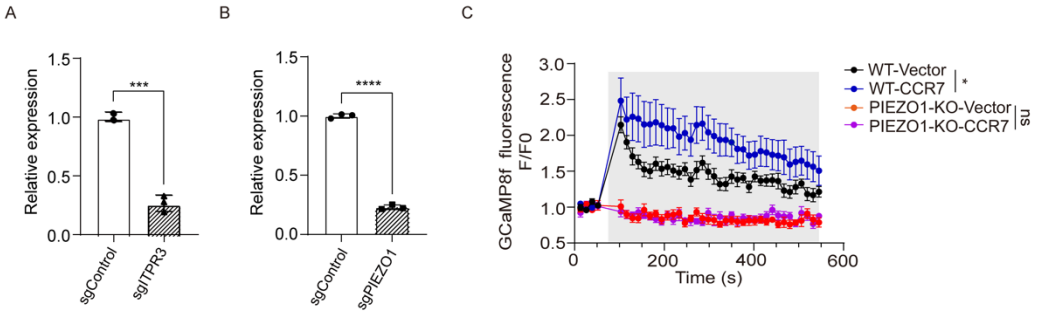

Figure S3. CCR7 regulates osmomechanical calcium signaling through PIEZO1

(A-B) Validation of CRISPRi-mediated knockdown efficiency. Relative mRNA expression of *ITPR3* (A) and *PIEZO1* (B) in HEK293T cells expressing sgControl or gene-specific sgRNAs, measured by qRT-PCR. Data are mean ± SD (n = 3). **P < 0.01, ***P < 0.001, ****P < 0.0001; unpaired two-tailed Student's t-test.

(C) *CCR7* overexpression fails to restore calcium influx in *PIEZO1*-knockout cells. GCaMP8f traces of WT or PIEZO1-KO cells transfected with vector or *CCR7* are shown alongside sgControl-Vector cells, measured by microplate reader. Traces represent mean $\Delta F/F_0$ ± SEM (n = 5). Gray shading indicates stimulation. ns, not significant, *P < 0.05; one-way ANOVA.

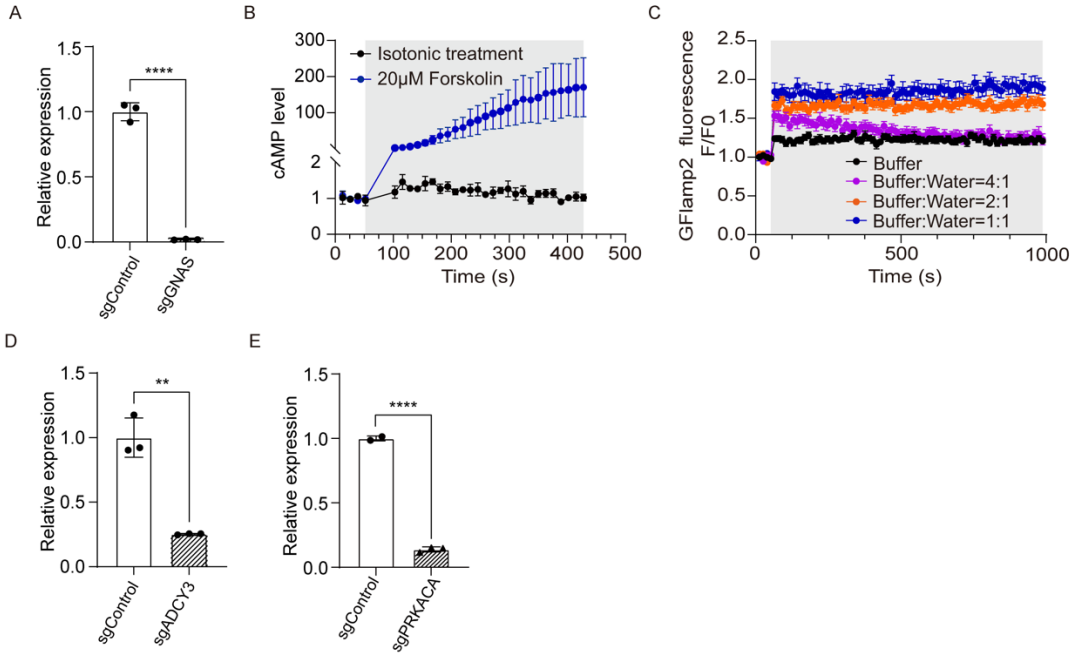

Figure S4. CCR7 modulates osmomechanical calcium signaling through the Gαs-cAMP-PKA Pathway

(A) Validation of CRISPRi-mediated knockdown efficiency. Relative mRNA expression of *GNAS* in HEK293T cells expressing sgControl or *GNAS*-targeting sgRNA (sgGNAS), measured by qRT-PCR. Data are mean ± SD (n = 3). ****P < 0.0001; unpaired two-tailed Student's t-test.

(B) Forskolin activates adenylyl cyclase and increases intracellular cAMP levels. HEK293T cells expressing the cAMP biosensor GloSensor-22F were treated with isotonic buffer or 20 μM forskolin. Traces show mean cAMP levels ± SEM (n = 2 or 3), measured by microplate reader. Gray shading indicates treatment period.

(C) Hypotonic stimulation increases intracellular cAMP levels in an osmolarity-dependent manner. HEK293T cells expressing the genetically encoded cAMP sensor GFlamp2 were subjected to varying degrees of hypotonic stimulation (buffer:water ratios of 4:1, 2:1, and 1:1). Traces show mean fluorescence intensity (F/F_0) ± SEM (n = 10), measured by microplate reader. Gray shading indicates stimulation period.

(D-E) Validation of CRISPRi-mediated knockdown efficiency. Relative mRNA expression of *ADCY3* (D) and *PRKACA* (E) in HEK293T cells expressing sgControl or gene-specific sgRNAs, measured by qRT-PCR. Data are mean ± SD (n = 3). **P < 0.01, ****P < 0.0001; unpaired two-tailed Student's t-test.